Technical Report

UDC 669 . 1 : 681 . 3

Visualizing and Monitoring Technology for Steel Production Processes

Masahiro ITO* Masataka INOUE

Abstract

Steel production involves many processes that monitor spatial distribution, and various measuring sensors have been developed and installed in a large number of facilities to monitor the operation status. We outline the image information technology of steel production process data by correlating the installed position of each sensor and the measured value at the facility, and reveal statistical and local uneven distribution information latent to image information data and their mathematical backgrounds. We also examine various cases of operating condition monitoring technology.

1. Introduction

In steel production processes, monitoring involves a recognition of spatial distribution in the operational state, and various measuring sensors have been developed to date and installed in a large number of facilities to monitor the operation status. We have developed image information technology of the operation data in the steel production process to grasp and predict unusual behavior of the steel production process in which numerous measuring data are comprehensively evaluated both spatially and temporally, the success of which has conventionally relied on the experience and skill of operators.[1, 2]

This paper briefly describes the image information technology in the steel production process data developed so far, and the mathematical background and examination cases of the technology that monitors the operation condition by revealing statistical and local unevenly distributed information latent in the image information data.

2. Image Information of Steel Production Process Data

2.1 Contour line search method of blast furnace process operation data

A blast furnace has various measuring sensors such as furnace body thermometers, furnace pressure gauges, top gas component analyzers, etc. to monitor operation and to control the equipment. For example, about 350 thermometers including a stave thermometer, furnace hearth wall thermometer, and furnace bottom thermometer are installed to determine the temperature distribution of the entire furnace. The furnace pressure gauges are installed in the furnace peripheral direction of each 90° or 45° angle at the shaft and at multiple levels in the height direction to perform monitoring together with the top gas pressure gauge and the blower pressure gauge.

Currently, the measuring sensors installed on the furnace body cannot always be placed evenly in terms of space. Therefore, the values of the zone where measuring sensors are not installed are spatially interpolated to find the contour line in a 3-D space.

The concept of this method is shown in **Fig. 1**. The furnace body consists of a furnace opening, furnace shaft, furnace barrel, bosh, and hearth. At Area A in Fig. 1, the position of the thermometer placed at the stave consisting of the furnace shaft as an example is indicated by ●. Now, the virtual grid of the space resolution necessary for evaluation of the furnace body temperature distribution, which is denser than the layout density of the stave thermometers, is set to the furnace body, and the temperature of the virtual grid point is spatially interpolated by the measurement value of the stave thermometer for calculation. Figure 1 shows the virtual grid point by ○.

At this time, 3-D coordinates (θ_p, r_p, h_p) of virtual grid point p in Area A are already known and the adjacent four stave thermometers a, b, c and d in the form of surrounding virtual grid point p are selected according to the 3-D Euclidean distance calculation using this coordinate. The coordinates and temperatures T_a (θ_a, r_a, h_a), T_b (θ_b, r_b, h_b), T_c (θ_c, r_c, h_c) and T_d (θ_d, r_d, h_d) of each stave thermometer are already known.

At this time, unknown temperature T_p in virtual grid point p can calculate the positions of the four thermometers above with the linear interpolation formula by projecting them onto the 2-D plane in

* Senior Manager, Systems & Control Technology Dept., Systems & Control Engineering Div., Plant Engineering and Facility Management Center
20-1 Shintomi, Futtsu City, Chiba Pref. 293-8511

the furnace peripheral direction ($r\cdot\theta$) and furnace height direction (h). It can be calculated by Formula (1) substituting (2) below.

$$T_p = T_{m2} + \frac{h_p - h_{m2}}{h_{m1} - h_{m2}} \cdot (T_{m1} - T_{m2}) \tag{1}$$

$$\begin{cases} T_{m1} = T_a + \dfrac{r_p\cdot\theta_p - r_a\cdot\theta_a}{r_b\cdot\theta_b - r_a\cdot\theta_a} \cdot (T_b - T_a) \\ T_{m2} = T_d + \dfrac{r_p\cdot\theta_p - r_d\cdot\theta_d}{r_c\cdot\theta_c - r_d\cdot\theta_d} \cdot (T_c - T_d) \\ h_{m1} = h_a + \dfrac{r_p\cdot\theta_p - r_a\cdot\theta_a}{r_b\cdot\theta_b - r_a\cdot\theta_a} \cdot (h_b - h_a) \\ h_{m2} = h_d + \dfrac{r_p\cdot\theta_p - r_d\cdot\theta_d}{r_c\cdot\theta_c - r_d\cdot\theta_d} \cdot (h_c - h_d) \end{cases} \tag{2}$$

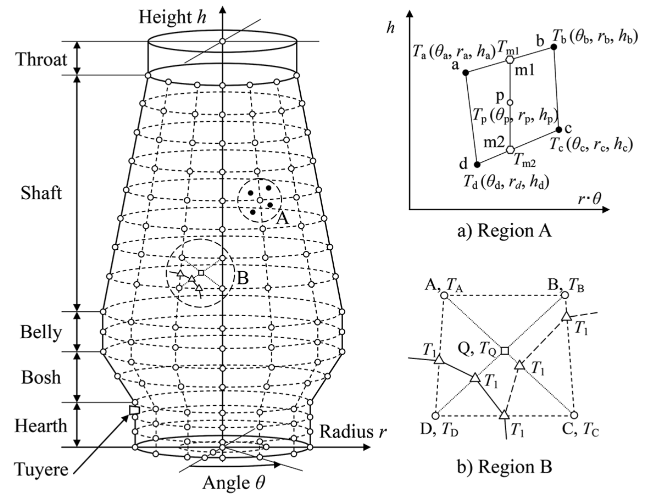

Fig. 1 Concept of deciding a measuring data contour line on blast furnace

When these calculations are performed at all virtual grid points, the spatial distribution calculation of the furnace body temperature is completed by considering the position of the thermometer accurately.

When four virtual grid points A, B, C and D with specified values in Area B of Fig. 1 are available and the temperature is T_A, T_B, T_C and T_D, respectively, the diagonal intersection point (□ in the figure) of the rectangular element ABCD of the virtual grid is assumed to be Q. Temperature T_Q in point Q is calculated by the arithmetic mean of four peak temperatures, i.e. Formula (3).

$$T_Q = \frac{1}{4} \cdot (T_A + T_B + T_C + T_D) \tag{3}$$

If one of the interior angles in rectangular element ABCD of the virtual grid does not exceed 180°, the inside of rectangular element ABCD can be divided into four triangular elements (ABQ, BCQ, CDQ and DAQ) with diagonal intersection Q at the peak.

Using the peak values of the four triangular elements calculated using the procedures above, assuming that the temperature in each triangular element can be determined by linear interpolation of the value at the side end, the coordinates on the side of each triangular element having the value of temperature T_1 to be searched can be determined. Connecting these points can lead to search of the T_1 contour line.

Finally, since the triangular element is used, the problem of contour line intersection or breaking half-way is eliminated. Coordinate calculations consisting of contour lines can be uniquely determined by simple algebra (linear interpolation calculation on the side using the value of the side end) and contour line search processing can be performed at high speed.

2.2 Image information of blast furnace process operation data

Figures 2 and **3** show examples of image information of the blast furnace process operation data. The 3-D is prepared by the perspective projection method setting the viewpoint and the vanishing point. In a) in Fig. 2, the furnace body shows the shaft pressure dis-

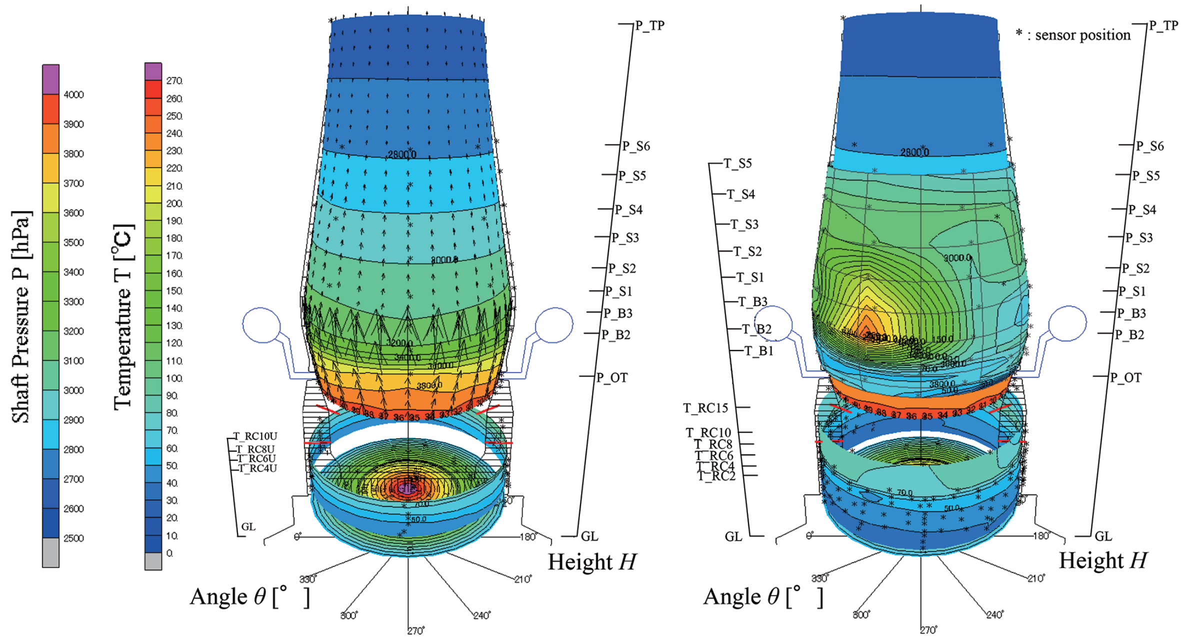

a) Shaft pressure, hearth wall (inside) and hearth temperature b) Shaft pressure, stave, hearth wall (outside) and hearth temperature

Fig. 2 3-Dimensional image of blast furnace process data (#2BF Oita Works, Nippon Steel & Sumitomo Metal)

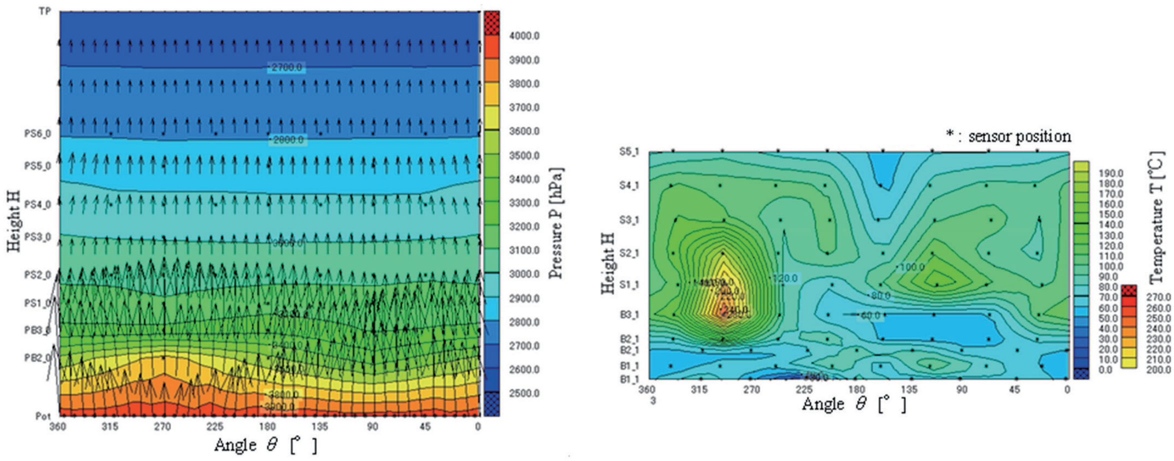

a) Shaft pressure b) Stave temperature

Fig. 3 2-Dimensional image of blast furnace process data (#2BF Oita Works, Nippon Steel & Sumitomo Metal)

tribution overlapping the space variation rate vector diagram of the shaft pressure, and the furnace lower part shows the hearth wall temperature (inside) distribution and the furnace bottom temperature distribution. In b) in Fig. 2, the furnace body shows the shaft pressure distribution overlapping the stave temperature distribution, and the furnace lower part shows the hearth wall temperature (outside) distribution and the furnace bottom temperature distribution.

Figures 2 and 3 show that the temperature distribution or pressure distribution of the blast furnace process can be objectively known or shared, and does not depend on the experience or skill of operators.

For the space variation ratio vector of the shaft pressure, the space variation ratio component of the shaft pressure is calculated in the furnace periphery/furnace height tangent direction at each virtual grid point and vectors consisting of these two components are defined. The size is equivalent to the volume for which conventional ventilation index $\Delta P/L$ Pa/m is spatially expanded.

2.3 Operation data image information of variable width mold in continuous casting process[3)]

In the following section, as an example of the steel process image information for which the image information area is temporally changed, the variable width mold operation data image information technology in the continuous casting process is described.

Figure 4 shows the outline of the variable width mold and **Fig. 5** shows the coordinate system and the mold dimensions. **Figure 6** shows the enlarged moving process of the mold short side surface BFGC to B'F'G'C'. The temperature measuring point (○ in the figure) in the variable width mold is not always evenly placed, but in Fig. 6, temperature measuring points a and b are placed on the mold long side surface, and temperature measuring points c and d are placed on the short side surface.

The placement position of each temperature measuring point is already known from the equipment drawing. Temperature measuring points c and d are fixed to the short side surface BFGC and they move along with the short side surface BFGC. The 3-D coordinates of temperature measuring points c' and d' moving on the short side surface are calculated every moment using the position information (for example, C or G, and C' or G' coordinates in Fig. 6) of the short side surface and the mechanical structure (for example, taper angle α rad in Fig. 6).

1) Before variation of casting width: Temperature calculation of

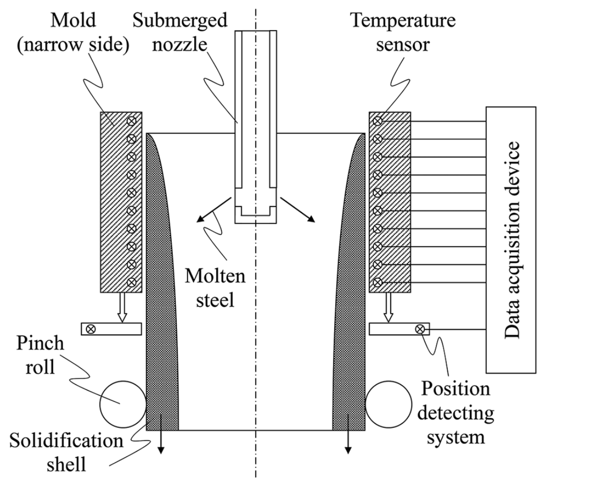

Fig. 4 Configuration diagram of a continuous casting machine variable width mold

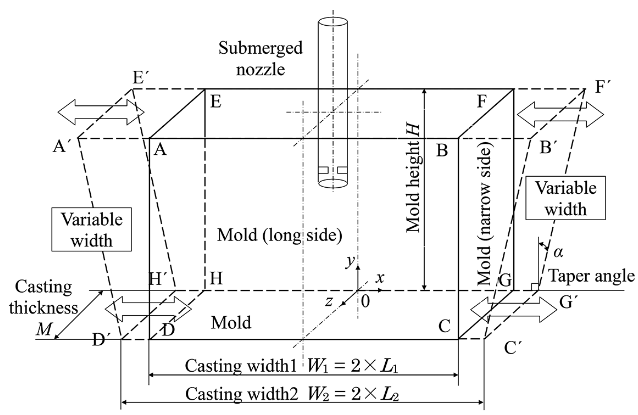

Fig. 5 Explanation of continuous casting machine variable width mold

point p and point q on connecting line BC

In Figs. 5, 6, casting width 1 before variation of the casting width is determined as $W_1 (= 2 \times L_1)$, the casting thickness as M and the origin of the coordinate axis as the end of the mold center lower end. The coordinates a(X_a, Y_a, Z_a) and c(X_c, Y_c, Z_c) of temperature measuring points a and c and temperatures T_a and T_c are already known.

Where, considering plane XY, which has developed mold long side surface ABCD and short side surface BFGC (**Fig. 7**), point p on connecting line BC is on line ac. Coordinate p(X_p, Y_p, Z_p) of point p can be defined by Formula (4·1) to Formula (4·3).

$$X_p = L_1 \tag{4·1}$$

$$Y_p = Y_a + \frac{Y_c - Y_a}{L_1 + M - Z_c - X_a} \cdot (X_p - X_a) \tag{4·2}$$

$$Z_p = M \tag{4·3}$$

Since point p corresponds to m1 shown in the blast furnace of Fig. 1, the value of temperature T_p can be calculated by the linear interpolation formula, Formula (5), similar to Formula (1) and Formula (2).

$$T_p = T_a + \frac{T_c - T_a}{L_1 + M - Z_c - X_a} \cdot (X_p - X_a) \tag{5}$$

Also, the values of coordinate q(X_q, Y_q, Z_q) and temperature T_q of point q on connecting line BC can be calculated by Formula (6·1) to Formula (6·3) and Formula (7) in a similar way.

$$X_q = L_1 \tag{6·1}$$

$$Y_q = Y_b + \frac{Y_d - Y_b}{L_1 + M - Z_d - X_b} \cdot (X_q - X_b) \tag{6·2}$$

$$Z_q = M \tag{6·3}$$

$$T_q = T_b + \frac{T_d - T_b}{L_1 + M - Z_d - X_b} \cdot (X_q - X_b) \tag{7}$$

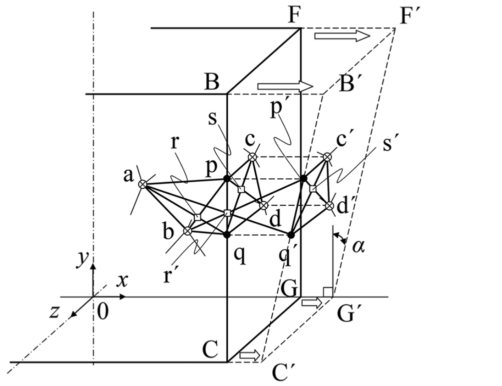

Fig. 6 Temperature measurement points in casting width variable process

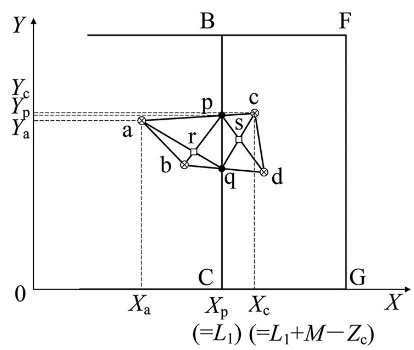

Fig. 7 Temperature measurement points on developed mold corner plane (before changing casting width)

According to measuring temperatures T_a, T_b, T_c and T_d and calculation temperatures T_p and T_q, temperatures T_r and T_s of diagonal intersection points r and s of rectangular zones apqb and cpqd are obtained by the arithmetic mean formula as in Formula (3).

$$T_r = \frac{1}{4} \cdot (T_a + T_p + T_q + T_b) \tag{8}$$

$$T_s = \frac{1}{4} \cdot (T_c + T_p + T_q + T_d) \tag{9}$$

2) Casting width variation process: Temperature calculation of point p' and q' on connecting line B'C'

In casting width 2 in the casting width variation process, W_2 (= 2 × L_2), casting thickness M, coordinates a(X_a, Y_a, Z_a) and c'$(X_{c'}, Y_{c'}, Z_{c'})$ of temperature measuring point a and point c' and temperatures T_a and $T_{c'}$ are already known.

Assuming that the concept of developed plane XY in Fig. 7 is expanded and that expanded plane XY develops mold long side surface A'B'C'D' and short side surface B'F'G'C' (**Fig. 8**), coordinates p'$(X_{p'}, Y_{p'}, Z_{p'})$ and q'$(X_{q'}, Y_{q'}, Z_{q'})$ and temperatures $T_{p'}$ and $T_{q'}$ of point p' and point q' on connecting line B'C' can be defined and calculated by Formula (10) to Formula (15) in a similar way.

$$X_{p'} = L_2 \tag{10·1}$$

$$Y_{p'} = Y_a + \frac{Y_c \cdot \cos\alpha - Y_a}{L_2 + Y_c \cdot \sin\alpha + M - Z_{c'} - X_a} \cdot (X_{p'} - X_a) \tag{10·2}$$

$$Z_{p'} = M \tag{10·3}$$

$$T_{p'} = T_a + \frac{T_{c'} \cdot \cos\alpha - T_a}{L_2 + Y_c \cdot \sin\alpha + M - Z_{c'} - X_a} \cdot (X_{p'} - X_a) \tag{11}$$

$$X_{q'} = L_2 \tag{12·1}$$

$$Y_{q'} = Y_b + \frac{Y_d \cdot \cos\alpha - Y_b}{L_2 + Y_d \cdot \sin\alpha + M - Z_{d'} - X_b} \cdot (X_{q'} - X_b) \tag{12·2}$$

$$Z_{q'} = M \tag{12·3}$$

$$T_{q'} = T_b + \frac{T_{d'} \cdot \cos\alpha - T_b}{L_2 + Y_d \cdot \sin\alpha + M - Z_{d'} - X_b} \cdot (X_{q'} - X_b) \tag{13}$$

$$T_{r'} = \frac{1}{4} \cdot (T_a + T_{p'} + T_{q'} + T_b) \tag{14}$$

$$T_{s'} = \frac{1}{4} \cdot (T_{c'} + T_{p'} + T_{q'} + T_{d'}) \tag{15}$$

From the development perspective, axis X in Fig. 8 is a polyline corresponding to taper angle α in C'. Here, considering that the calculation formula of coordinates and temperatures at each point is linear interpolation in plane XY developed using the Mercator pro-

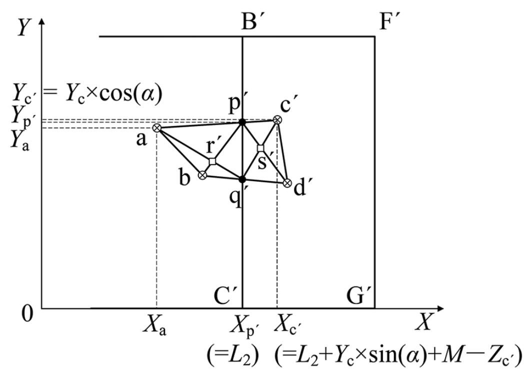

Fig. 8 Temperature measurement points on developed mold corner plane (under changing casting width)

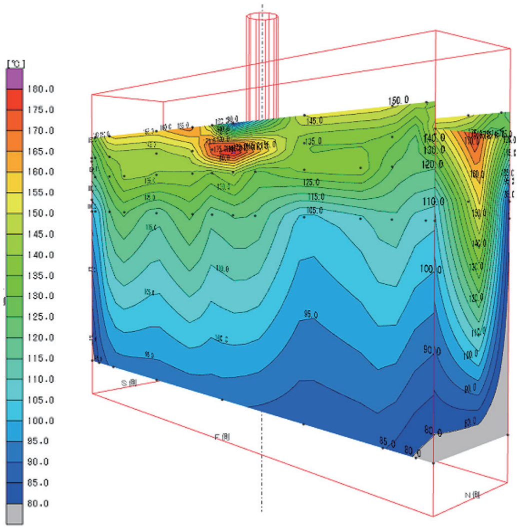

Fig. 9 3-Dimensional image of continuous casting machine variable width mold temperature (#1CC Yawata Works, Nippon Steel & Sumitomo Metal)

jection method, the same development perspective as that in Fig. 7 is shown. When $\alpha = 0$ and $L_2 = L_1$, Formula (10) to Formula (15) are equal to Formula (4) to Formula (9).

From Formula (8) and Formula (9), temperatures T_r and T_s of the diagonal cross-section point in rectangular zone apqb and cpqd before the casting width variation are obtained. From Formula (14) and Formula (15), temperatures $T_{r'}$ and $T_{s'}$ of the diagonal cross-section point in rectangular zone ap'q'b and cp'q'd in the casting width variation process are obtained. If one of the inner angles in these rectangular zones is associated with the rectangular element that does not exceed 180°, the image information area can be drawn even in the changing casting width variation process with time by periodic search of the contour line. Even in the mold corner where it is difficult to grasp the status of the initial solidification due to the effect of molten steel rotational flow or other effects, the temperature distribution can be spatially known and change with time can be monitored using the thermometer measurement value nearby.

Figure 9 shows an example of image information of operation data in the continuous casting machine variable width mold.

3. Operating Condition Monitoring Technology of Steel Process

3.1 Basic concept

In monitoring the operating condition, image information of the steel process data means that multi-dimensional vectors for each measuring sensor, each virtual grid point or each pixel are handled based on the distribution constant characteristics of the steel production process.

The steel production process has many processes based on continuous operation. Much of this information data can be collected. Attention has focused on statistical analysis based on normal distribution, so-called big data analysis or the recent AI method with image input.

At this time, operating condition monitoring required for the steel production process is conducted to clarify local/non-steady characteristics that are inherent/latent unsteady behavior in the operation condition, low in quantity, from a steady and stable large amount of operation data that occupies the most part statistically and temporally. It is important to find potential characteristics that cannot be found by the principal composition analysis that is generally and widely used as multivariate analysis.

The steel production process basically attempts to realize and achieve steady and stable status. The analysis (for example, principal composition analysis) that selects steady characteristics occupying the most part statistically or temporally is effective for optimization of the operating conditions as static characteristics. In a) monitoring of non-steady characteristics as dynamic characteristics resulting in process malfunction or b) monitoring of unevenly distributed characteristics latent in spatial location, the independent composition analysis focusing on the blind signal separation[4)] is considered effective for the former, and sparse modeling[5, 6)] generated from the information processing study of the biological visual system is considered effective for the latter.

The following shows the mathematical background and the review example.

3.2 Operating condition monitoring model of steel production process data with image information

Figure 10[7)] shows the relationship between the signal generated in the brain and the observation signal in the magnetoencephalogram analysis. Inside the mold of the blast furnace process or continuous casting process, there are multiple heat sources or pressure sources with local or spatial distribution arising from physical phenomena such as phase change or chemical reaction. The temperature or pressure after conducting/flowing inside from these sources is considered to be the measurement value of the sensor installed in the equipment.

In Fig. 10, $s_1(t)$ and $s_2(t)$ are source signals, while $x_1(t)$, $x_2(t)$, …, and $x_5(t)$ are observation signals. Each signal is expressed in vector notation as $\mathbf{s}(t) = (s_1(t), s_2(t), \ldots, s_n(t))^T$ and $\mathbf{x}(t) = (x_1(t), x_2(t), \ldots, x_m(t))^T$. Defining matrix **A** of row m and column n, having a_{ij} as the (i, j) element, it is assumed that these relationships can be expressed in the following formula:

$$\mathbf{x}(t) = \mathbf{A} \cdot \mathbf{s}(t) \qquad (16)$$

Formula (16) is a model in which observing signal $\mathbf{x}(t)$ is represented by a linear combination of source signal $\mathbf{s}(t)$ and matrix **A**. In this case, a_{ij} is a linear combination coefficient from source signal j to sensor i ($x_i(t) = \Sigma_{j=1}^{n} a_{ij} \cdot s_j(t)$). If the nonlinearity and dynamics of matrix **A** are small enough to be disregarded, principal component analysis, independent component analysis, and sparse modeling can be viewed as analytical methods by which to derive matrix **A** that

$$x_1(t) = a_{11} \cdot s_1(t) + a_{12} \cdot s_2(t)$$
$$x_2(t) = a_{21} \cdot s_1(t) + a_{22} \cdot s_2(t)$$
$$\ldots$$
$$x_5(t) = a_{51} \cdot s_1(t) + a_{52} \cdot s_2(t)$$

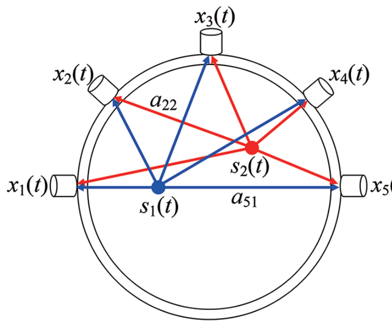

Fig. 10 Generating signals inside brain and observing signals[7)]

constitutes Formula (16) (or realistically, recovery matrix **W** below) using each evaluation function and to clarify source signal $\mathbf{y}(t)$ using Formula (17).*1

$$\mathbf{y}(t) = \mathbf{W} \cdot \mathbf{x}(t) \quad (17)$$

3.3 Evaluation functions of principal component analysis, independent component analysis, and sparse modeling

Described below are the evaluation functions of the three analytical methods and recovery matrix **W**.

When the mean of source signal $y_j(t)$ is non-zero ($E\{y_j(t)\} \neq 0$), k-th order moments around the mean κ_{kj} are as follows:[8)]

$$\kappa_{1j} = E\{y_j\} \quad (18\cdot1)$$

$$\kappa_{2j} = E\{y_j^2\} - [E\{y_j\}]^2 \quad (18\cdot2)$$

$$\kappa_{3j} = E\{y_j^3\} - 3E\{y_j^2\}E\{y_j\} + 2[E\{y_j\}]^3 \quad (18\cdot3)$$

$$\kappa_{4j} = E\{y_j^4\} - 3[E\{y_j^2\}]^2 - 4E\{y_j^3\}E\{y_j\} + 12E\{y_j^2\}[E\{y_j\}]^2 - 6[E\{y_j\}]^4 \quad (18\cdot4)$$

If the mean of $y_j(t)$ is set to zero in the previous calculation, the result will be $E\{y_j(t)\} = 0$.

1) Evaluation function of principal component analysis and recovery matrix **W**

Evaluation function: second moment (variance) to be maximized

$$\kappa_{2j} = E\{y_j^2\}(= \sigma_{yj}^{\,2}) \quad (19)$$

Recovery matrix **W** consisting of orthogonal direction vector $\mathbf{w}_j$, which statistically contains a large amount of data

2) Evaluation function of independent component analysis and recovery matrix **W**

Evaluation function: higher-order moment to be maximized or minimized

For example, fourth moment (kurtosis) to be maximized or minimized (Fast ICA)[8, 9)]

$$\kappa_{4j} = E\{y_j^4\} - 3[E\{y_j^2\}]^2 \quad (20)$$

Recovery matrix **W** consisting of direction vector $\mathbf{w}_j$, which is statistically independent

3) Evaluation function of sparse modeling and basis matrix **Φ**

Evaluation function: basic matrix **Φ**, which makes up zero elements, to be optimized[10)]

$$\min_{\mathbf{x}\in R^m} \|\mathbf{x}\|_0 \ \textit{subject to}\ \mathbf{y} = \mathbf{\Phi} \cdot \mathbf{x} \quad (21)$$

Basic matrix **Φ***2 consisting of orthogonal function φ_j to extract local deviance from main space components

3.4 A case of blast furnace process operating condition monitoring using independent component analysis

At the No. 4 blast furnace at the Kimitsu Works of Nippon Steel & Sumitomo Metal Corporation, we conducted independent component analysis on two-dimensional image information of shaft pressure - furnace peripheral angle (θ) and furnace height (h). Data were taken for one year from 00:00 on August 1, 2004 until 23:55 on July 31, 2005, at a sampling cycle of five minutes and pixel number of 105 120 (= k).

An equally spaced 14 × 14 grid was assigned to each image to extract a value (**Fig. 11**), which was then rearranged in numerical order to create 196 (= m) order observing signal vector $\mathbf{x}(t)$ and observing signal matrix $\mathbf{X} \in R^{m\times k}$. The number of independent components n was set to n = 5 as a number that allows physical interpretation of the basic image.

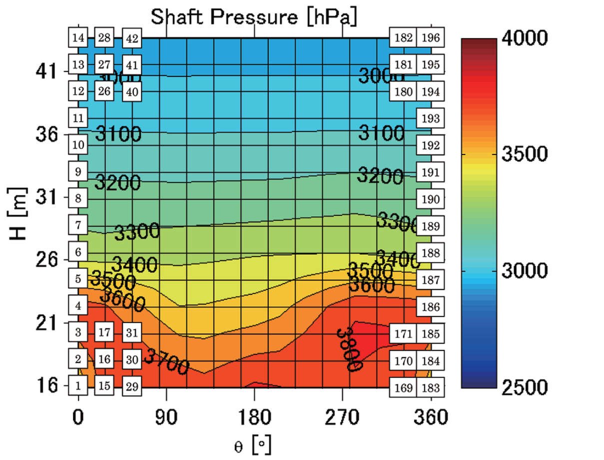

Fig. 11 Mesh and element number of observing signal vector x(*t*) on image

$$\mathbf{X} = \mathbf{A} \cdot \mathbf{S} \quad (22)$$

$$\mathbf{X} = [\mathbf{x}(1)\ \ \mathbf{x}(2)\ \ \cdots\ \ \mathbf{x}(k)] \in R^{m\times k} \quad (23)$$

$$\mathbf{S} = [\mathbf{s}(1)\ \ \mathbf{s}(2)\ \ \cdots\ \ \mathbf{s}(k)] \in R^{n\times k} \quad (24)$$

For simplification purposes, **A** and **S** are herein defined as $\mathbf{A} = \mathbf{W}^{-1}$ and $\mathbf{S} = \mathbf{Y}$. **Figure 12** shows an example of how independent component signal $s_j(t)$ fluctuates before and after blast volume reduction action is taken to prevent operational malfunction. Images in Fig. 12 are basic images of shaft pressure A_1 to A_5, from the top. Based on the contour lines of each image, the following interpretation is made:

Basic image A_1: Basic image of furnace ventilation characteristics
Basic image A_2: Image of bosh section gas flow components above the tuyere
Base image A_3: Image of gas drift components near 100°
Basic image A_4: Image of gas drift components near 0°
Basic image A_5: Image of gas drift components near 300°

In this case, the basic image is an image obtained by rearranging the column component of matrix **A**, which corresponds to independent component signal $s_i(t)$, in the grid position in Fig. 11.

Figure 12 is a case of blast volume reduction executed at 9:20 on September 30 (A in Fig. 12), as a result of differential pressure in the furnace middle section shifting to higher levels during normal operation monitoring, followed by the occurrence of three slips. Considering that iron ore stays in the furnace for about 10 hours, a dotted line is added as a guide to the time 48 hours before blast volume reduction.

Analysis of Fig. 12 from the viewpoint of operation monitoring based on time-series transitions of independent component signals reveals that at around 3:00, on September 29, approximately 30 hours before the blast volume reduction, there occurred significant fluctuations in independent component signal $s_j(t)$, which corresponds to the basic images of shaft pressure A_1 and A_3 (B4 and B3 in Fig. 12, respectively). Also fluctuation in differential pressure ΔP (blast pressure P_B − furnace top pressure P_{TP}), which is a conventional operation index, can be confirmed (as seen in D in Fig. 12) but to a lesser extent. Differential pressure ΔP is merely an overall indicator of furnace ventilation and presents little information regarding the in-furnace condition.

Thus, time-series transitions of the independent component sig-

*1 Ideally, when $\mathbf{W} \cdot \mathbf{A} = \mathbf{I}$, $\mathbf{A} = \mathbf{W}^{-1}$ and $\mathbf{s} = \mathbf{y}$ can be uniquely determined. Depending on the method, an arbitrary property is still found in the scaling and symbol of the original signal vector and in the composition sequence.

*2 Status quantity $I(x, y) = \Sigma_{j=1}^{n} a_j \cdot \Phi_j(x, y)$ of 2-D pixel (x, y) and formulation.[5, 6, 10)]

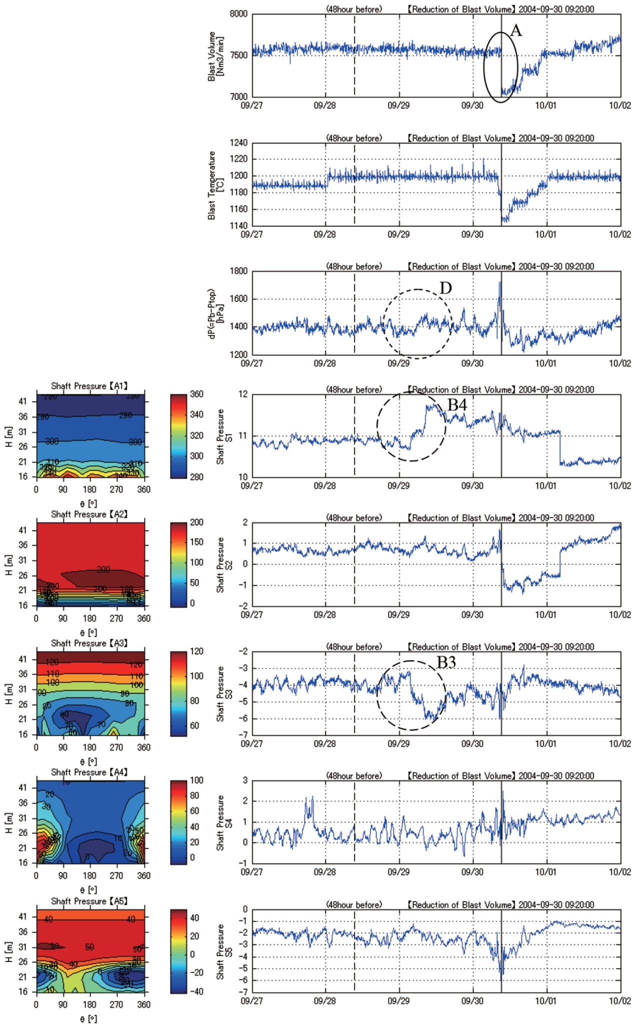

Fig. 12 Results of ICA for shaft pressure image

nal $s_j(t)$ clearly indicate a fluctuating distribution base, extract and quantify fluctuations, and therefore are considered effective in operation monitoring.

4. Conclusions

This paper describes the image information technology of steel production process data we have developed. It also presents mathematical backgrounds and examination cases of operating condition monitoring technology by revealing statistical and local uneven distribution information latent in a large amount of image information data.

Figures 1, 2, 3, 11, and 12 and their explanations in this paper are quoted from the referenced literature 2) with the reprint permission of the Society of Instrument and Control Engineers.

References

1) Ito, M. et al.: Shinnittetsu Giho. (379), 33 (2003)
2) Ito, M. et al.: SICE Transactions on Industrial Application. 8 (10), 82 (2009)
3) Japan Patent Publication No. 4980388. April 27, 2012
4) Jutten, C. et al.: Signal Processing. 24 (1), 1 (1991)
5) Olshausen, B.A. et al.: Nature. 381, 607 (1996)
6) Olshausen, B.A. et al.: Network. 7 (2), 333 (1996)
7) Murata, N.: Independent Component Analysis. First Edition. Tokyo, Tokyo Denki University Press, 2004, p. 23, 205
8) Written by Hyvärinen, A. et al., Translated by Nemoto, I. et al.: Independent Component Analysis. First Edition. Tokyo, Tokyo Denki University Press, 2005, p. 45, 197, 426
9) Hyvärinen, A. et al.: Neural Computation. 9, 1483 (1997)
10) Nagahara, M.: Sparse Modeling. First Edition. Tokyo, Corona Publishing, 2017, p. 9

Masahiro ITO
Senior Manager
Systems & Control Technology Dept.
Systems & Control Engineering Div.
Plant Engineering and Facility Management Center
20-1 Shintomi, Futtsu City, Chiba Pref. 293-8511

Masataka INOUE
Manager
Systems & Control Technology Dept.
Systems & Control Engineering Div.
Plant Engineering and Facility Management Center